Evaluation Of Fracture Energy Of Concrete By Hybrid SVR Analysis

Pan JIANG[1*] and Nan GE[2]

[1] Department of Civil Engineering, Hebei University of Water Resources and Electric Engineering, Cangzhou 061001, China
[2] College of Civil and Architectural Engineering, North China University of Science and Technology, Tangshan 063210, China
[*] Corresponding author. E-mail: jiangpan123321@126.com

Received: Jul. 13, 2023; Accepted: Dec. 10, 2023

Regression techniques were developed to determine the concrete initial (G_f) and total (G_F) fracture energy based on prior data using mechanical features and mixed design elements. There were 264 samples retrieved from prior investigations in all. Research contributes to the field by improving the accuracy of predicting concrete fracture energy, offering a methodology for optimizing hyperparameters, and providing a model comparison that demonstrates the practical value of the new approach. These findings can benefit the construction and engineering industries by enhancing the accuracy of material property predictions and improving the quality and safety of constructed structures. This study merged support vector regression (SVR) assessment with arithmetic optimization algorithm (AOA) and whale optimization algorithm (WOA) to predict the G_f and GF_F of concrete. The aim of combining the optimization algorithms with SVR analysis was to determine the optimal values of hyperparameters that play pivotal role in developed models' accuracy. The computation and analysis for G_f and G_F using five criteria shows that optimized SVR-AOA and SVR-WOA analyses can do admirably well throughout the forecasting model. When the outperforming SVR analysis was compared to the library, it was discovered that the newly constructed SVR-AOA also present a small raise in accuracy, with modification in all metrics. In conclusion, while the SVR-WOA demonstrates its effectiveness in the forecasting outline, the SVR-AOA analysis appears to be a reliable approach for determining accurate G_f values ($R^2_{train} = 0.921$, and $R^2_{test} = 0.9853$) and G_F values ($R^2_{train} = 0.9281$, and $R^2_{test} = 0.9236$), as supported by the arguments and feasibility of the models.

Keywords: Concrete; Fracture energy; Support vector regression; Optimization algorithms

http://dx.doi.org/10.6180/jase.202412_27(12).0005

Nomenclature

Please refer to Table 1 for the meanings of various symbols.

1. Introduction

Fracture mechanics approaches to design concrete samples to handle all sorts of brittle failures result in durable, cost-effective, and safer concrete structures [1, 2]. Many empirical and experimental research supported this hypothesis. In addition, construction mishaps show the necessity of fracture mechanics in concrete architecture [3]. Kaplan conducted the first linear elastic fracture mechanics (LEFM) laboratory experiment on concrete fracture mechanics [4]. Furthermore, Kesler et al. [5] illustrated the traditional LEFM of sharp cracks with just the fracture energy $\left(G_f\right)$, was insufficient for concrete buildings because of the presence of an inelastic region with extraordinary scale and full micro-cracks in front of the crack tip, named the fracture process zone (FPZ).

Researchers found two fracture factors needed to characterize concrete fracture [6]. Several studies were done to find the optimum FPZ nonlinear fracture model for concrete to reduce LEFM deficiencies [7]. Specific fracture energy is crucial to cohesive crack modeling. The work-of-

Table 1. Nomenclature

Nomenclature			
G_f	concrete initial fracture energy	G_F	concrete total fracture energy
SVR	support vector regression	AOA	arithmetic optimization algorithm
LEFM	linear elastic fracture mechanics	WOA	whale optimization algorithm
WFM	work-of-fracture method	FPZ	fracture process zone
f_{cm}	The average of f_c	f_c	compressive strength
w/c	the ratio of water to binder	d_{max}	Largest size of aggregate
CT	age of samples	α_0	$\alpha_0 = 1$ for rounded, $\alpha_0 = 1.44$ for crushed
ω	weighted vector	PCC	Pearson correlation coefficient
$\emptyset(X)$	the planning function	b	a constant
α_i and α_i^*	Lagrangian multipliers	ξ_i and ξ_i^*	positive loose variables
σ	kernel width	x_j and x_i	input in the j^{th} and i^{th} dimensions
UB_j	upper value of the j_{th} location	MOA	Math Optimizer Accelerated
μ	control parameter	LB_j	lower value of the j_{th} location
S	Subtraction	MOP	Math Optimizer probability
t	location vector of whales	A	Addition
A and C	coefficient vectors	$X_p(t)$	the location of the hunt
C	regularization	p	possibility number
R^2	Coefficient of determination	R	Correlation coefficient
RRSE	Root Relative Squared Error	RMSE	Root-mean-square error
m_d	The measurements	VAF	Variance account factor
z_d	The predictions	$\overline{m}$	The mean of measurements
D	Dataset's amount	$\bar{z}$	The mean of predictions

fracture (WFM) technique defined specific fracture energy as the effort needed to generate one crack unit. The fracture energy may be determined by dividing the total dissipated energy by the original ligament area, taking into account the division of the beam into two halves. The G_F obtained via WFM is specimen size and shape dependent [8]. However, early fracture energy $\left(G_f\right)$ is independent of sample size and shape and reflects the area under the first tangent of the softening curve [9]. Planas et al. estimate the G_F/G_f ratio as 2-2.5 [10]. G_F is needed to quantify energy consumption in total building collapse and anticipate the whole post-peak softening force-movement plot, whereas G_f is enough to estimate the greatest structural force and softening curves [11].

Traditionally, the load-displacement graph was used to accurately assess the fracture energy of concrete samples subjected to bending. From an experimental viewpoint, this is difficult and unintuitive. Developers and engineers have used quantitative or analytical methods to cut costs, time, and fracture energy measurements to uncover gaps in early fracture energy predictions. In recent decades, mathematical techniques have been developed to estimate the fracture characteristics of concrete built with different proportions, bypassing notched fracture specimens [3]. Conversely, standard methods cannot characterize complicated non-linear correlations. By a technique in a complex nonlinear design is difficult since finding a regression formula requires expertise and methods. Compared to current data analysis methods, new fulfilling, convenient, and exact processes are needed [12–16].

In recent times, the use of algorithms and soft computing approaches has been employed to enhance our comprehension of the mechanics of structure and materials [17–23]. Scholars have endeavored to create robust, accurate, and cost-effective models for predicting material properties by using available experimental data [24, 25]. Various machine intelligence methodologies have been used to forecast the detailed effectiveness of structural materials. The prediction of concrete fracture energy was accomplished by using a combination of Kriging, U-learning, and K-means clustering techniques, utilizing data obtained from prior experimental testing. The R-squared values for the suggested Kriging pairing hypotheses vary between 0.59 and 0.95 , but the R-squared values for the prior knowledge connections range from 0.14 to 0.69 . The findings illustrate that the combination of the Kriging approach, the U-learning function, and K-means clustering, together with a limited number of initial test results, leads to a reduction in testing time and cost, while simultaneously enhancing the accuracy of concrete fracture predictions [26].

SVR recognized a learning technique used for regression duties. Likewise of traditional methods, is particularly effective for dealing with non-linear and complex data relationships. The primary goal of SVR is to predict a continu-

ous target variable (e.g., a numerical value) based on input features. It's often used for tasks such as predicting stock prices, housing prices, or, as in the passage you provided, material properties like concrete fracture energy [27]. Like many machine learning algorithms, SVR has hyperparameters that need to be tuned [28, 29]. These include the choice of kernel, regularization parameter, and epsilon. Hyperparameter tuning is essential for achieving the best model performance. Various studies were considered this procedure for developing their model for prediction purposes. A hybrid SVR-grey wolf optimization (GWO) was developed for predicting the compressive strength of $GGBFS$-based geopolymer concrete [30], and bond strength of reinforced concrete [31], where hyperparameters of the SVR was tuned with GWO. Bayesian optimization algorithm-based SVR analysis was developed for estimation of shear capacity of FRP reinforced concrete members [32]. Shear strength of reinforced concrete deep beams was predicted by combining the SVR model with three novel metaheuristic optimization algorithms: African Vultures optimization algorithm ($AVOA$), particle swarm optimization (PSO), and Harris Hawks optimization (HHO) [33]. Mechanical properties of recycled aggregate concrete estimated using hybrid $PSO-SVR$ and $GWO-SVR$ models [34].

1.1. Main novelties and contributions

Various formulae for evaluating the fracture energy of concrete have been presented so far using informal statistical approaches [35]. Table 2 could be collected and presented for this purpose, corresponding to an enormous data collection.

The execution of high-quality research requires the allocation of resources such as time, financial investments, well-designed laboratory setups, meticulous planning, and the implementation of age-appropriate testing methodologies [39–41]. Human mistakes arising from insufficient skills and knowledge, researcher ineffectiveness during experimentation, and equipment failures may lead to both financial and temporal inefficiencies, as well as the generation of erroneous outcomes. The absence of essential equipment might provide a significant challenge to the assessment process. The use of simulation techniques for the determination of concrete fracture characteristics based on historical data has many benefits. The complex and nonlinear properties of concrete cannot be well captured by regressionbased methods often seen in codes and publications, such as empirical formulas. The assurance of user acceptance for the use of regression-based connections in identifying fracture traits is uncertain. Numerous researchers have examined various statistical assessment and estimating methodologies in order to identify and locate concrete fractures using test outcomes.

To achieve the desired objective function, it is essential to use an approximation approach that exhibits a high level of accuracy while relying on a restricted amount of starting data. This study suggested a coupled SVR methodology to have a greater effectiveness of concrete's G_f and G_F. Systems were utilized to estimate the G_f and G_F in this situation by integrating the arithmetic optimization algorithm (AOA) and whale optimization algorithm (WOA) approaches with SVR. Nevertheless, employing current data collection may be difficult at best. For this experiment, a data set was created that includes four data inputs and two outcome factors. At last, the performance of models has compared altogether and literature by calculating and analyzing different statistical criteria.

2. Data description

The selection of appropriate variables to input is a crucial stage in the use of regression analysis for the purpose of predicting fracture energy in concrete. Additional factors that may be utilized to ascertain fracture energy include porosity, grain size, presence of air voids, cement type, percentage of aggregate, and relative abrasiveness of the aggregate [42–44]. The aforementioned difficulties, however, tend to be disregarded as a result of a deficient comprehension of the methodologies used in the publications. Additional parameters, such as tensile strength and modulus of rupture, seem to contribute to the evaluation of fracture energy in concrete. However, calculating these quantities is difficult and strongly dependent on size influences [3]. Furthermore, since there is no available data on the weights of these variables, they are not featured in the research. Because samples with equal W/C but different f_c have different fracture energy, W/C must be entered individually. Based on physical considerations and the stated trend of fracture energy, as well as the basic form of the latest systems, four factors were considered: compressive strength (f_c), maximum aggregate size ($d_{\max}$), age of samples (CT), and water to cement ratio (W/C).

The G_f and G_F calculated by two sets of data, where collected from published articles [11, 45–67]. The collected dataset was passed some pre-processing efforts. The suggested partition for the examining and learning stages were 25% and 75%, respectively. Therefore, these percentages were used for data dividing for both G_f and G_F. It has been tried to both train and test stages includes the normal distribution, where this effort was performed by Randperm function. Next, the data row that could be have negative impact have been removed. Fig. 1 illustrates the distribu-

Table 2. The formulas created for assessing concrete fracture energy.

Eq. No.	Formula	Ref.
(1)	$G_f = \alpha_0 \left(\frac{f_c}{0.051}\right)^{0.46} \left(1 + \frac{d_a}{11.27}\right)^{0.22} \left(\frac{w}{c}\right)^{-0.3}$	[3]
(2)	$G_F = 2.5 G_f$	
(3)	$G_F = \left(0.0469 d_{max}^2 - 0.5 d_{max} + 26\right) \left(\frac{f_c}{10}\right)^{0.7}$	[36]
(4)	$G_F = 73 \left(f_{cm}\right)^{0.18}$	[37]
(5)	$G_F = 10 \left(d_{max}\right)^{0.33} \left(f_c\right)^{0.33}$	[38]
	: The mean of f_c : $\alpha_0 = 1$ for rounded, $\alpha_0 = 1.44$ for crushe	

tion of factors used in the computation of G_f for the A series and G_F for the B series. Table 3 presents a comprehensive depiction of the statistical data pertaining to the dependent and independent characteristics for the G_f and G_F model generation procedures.

In order to establish a connection between the two attributes, it is possible to construct and depict a correlation ratio referred to as the Pearson correlation coefficient (*PCC*). Table 4 presents the quantities of connections for attributes of G_f and G_F. The top surface, characterized by a brown color, of this table corresponds to the *PCC* values for G_f, whilst the lower surface, distinguished by a green color, represents the *PCC* values for G_F. If there is a substantial positive or negative *PCC*, experts can struggle to understand how the descriptive factors impact the outcomes. *PCC* values smaller than the required ones indicate that these features are probably generated by multicollinearity issues, with 0.374 and 0.475 suggested as the G_f and G_F boundaries, respectively. The greatest *PCC* for G_f is related to W/C and f_c with a value of -0.719 . Turning to G_f, the greatest *PCC* has resulted between W/C and f_c with the value of -0.662 and between G_F and f_c with a value of 0.539.

3. Base of applied methods

3.1. Support vector regression (SVR)

The *SVR* framework is capable of accommodating the number of predictor factors N and the number of elements in each x_i. This enables the framework to effectively address regression problems that include multiple predictors $X = \{x_i\}_{i=1}^{i=n}$. The target factor, denoted as $y = \{y_i\}_{i=1}^{i=N}$, is associated with the following factors [68]. The matrix X is transformed into a higher-dimensional feature space while maintaining its fundamental properties, albeit having a lesser input area. The problem at hand pertains to non-linear regression and is addressed by using a *SVR* technique [69]:

$$t = f(X) = \omega \cdot \emptyset(X) + b \tag{6}$$

In Eq. (1), ω, b, and $\emptyset(X)$ are the weighted vector, a constant, and the planning function utilized in the characteristic area. The following minimization procedure is used to assess the coefficients ω and b [69] :

$$\text{Minimize } \frac{1}{2}\|w\|^2 + C\frac{1}{N}\sum_{i=1}^{N}(\xi_i + \xi_i^*) \tag{7}$$

$$\text{Subject to } \begin{cases} | y_i - (w, x_i + b) \geq \varepsilon + \xi_i \\ \langle w, x_i \rangle + b - y_i \leq \varepsilon + \xi_i^* \\ \xi_i, \xi_i^* \geq 0 \end{cases} \tag{8}$$

The prescribed model parameters are C and ε [70]. The function's softness is measured by $\frac{1}{2}\|w\|^2$ and C analyzes the trade-off between experimental danger and softness. The parameters ξ_i and ξ_i^* are positive factors that represent the distance between real numbers and their associated border numbers in the framework's estimate of the ε-tube function.

A non-linear regression function may be constructed by the use of Lagrangian multipliers to optimize the given circumstances [69]:

$$f(x) = \sum_{i=1}^{i=N} (\alpha_i - \alpha_i^*) K(x_i, x_j) + b \tag{9}$$

The equation provided involves the variables α_i and α_i^* which represent Lagrangian multipliers. Additionally, $K\left(x_i, x_j\right)$ denotes the kernel that defines the inner product inside the D-dimensional feature space. It is important to note that x_i and x_j belong to the set X, representing the characteristics area [69]. Only a limited number of α_i and α_i^* coefficients will have non-zero values if the Kuhn-Tucker conditions are satisfied. The "support vectors" refer to the data points that are in closest proximity to the decision surface, also known as the hyperplane. The SVR model was constructed in this study using the radial basis function [71]:

$$K(x_i, x_j) = \exp\left(\frac{-\|x_i - x_j\|^2}{2\sigma^2}\right) \tag{10}$$

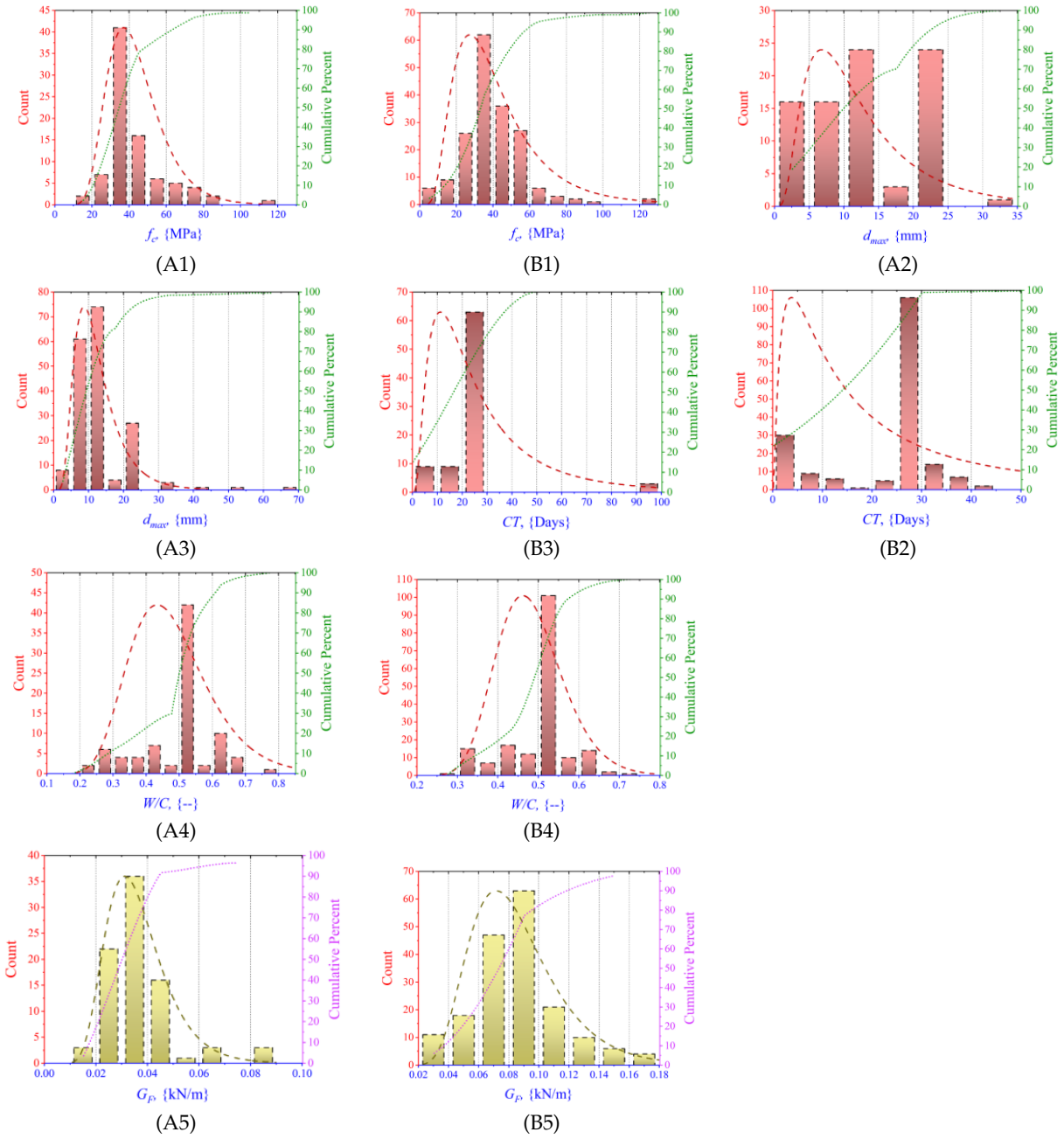

Fig. 1. Figures of variables: A series for G_f, B series for G_F.

The equation presented above involves the variables x_j and x_i, which represent the input in the j^{th} and i^{th} dimensions, respectively. Additionally, σ denotes the kernel width.

3.2. Arithmetic Optimization Algorithm (AOA)

The *AOA* method [72], as indicated in Eq. (11), begins with a set of nominee answers (X) that are generated accidentally, and in every iteration, the finest nominee answer is considered to be the finest produced answer or nearly the ideal until now [72].

$$X = \begin{bmatrix} x_{1,1} & \cdots & x_{1,j} & x_{1,n-1} & x_{1,n} \\ x_{2,1} & \cdots & x_{2,j} & \cdots & x_{2,n} \\ \vdots & \ddots & \vdots & \ddots & \vdots \\ x_{N-1,1} & \cdots & x_{N-1,j} & \vdots & x_{N-1,n} \\ x_{N,1} & \cdots & X_{N,j} & x_{N,n-1} & x_{N,n} \end{bmatrix} \tag{11}$$

The *MOA* feature, denoted as Math Optimizer Accelerated, is computed using Eq. (12) and is used in the primary

Table 3. The variables' characteristics.

Phase	Metrics	Inputs								Outputs			
		$f_c(MPa)$		$d_{\max}$(mm)		CT (days)		W/C		G_f	G_F		
		G_f	G_F	G_f	G_F	G_f	G_F	G_f	G_F	(kN/m)	(kN/m)		
Train													
	Max	87/2	124	32	65	90	40	0/8	0/65	0/1	0/178		
	Min	12/6	3.01	2	2	1	0/56	0.2	0/28	0/0	0/035		
	Med	39/9	38/5	12/7	10	28	28	0.5	0.5	0/0	0/084		
	Range	74/6	120/99	30/0	63	89/0	39/44	0.6	0.37	0/1	0/143		
	Skew	1/0547	1/642	0/252	3/557	3/0099	−1/089	−0/324	−0/789	1/986	0/828		
Test													
	Max	110	90	20	20	90	36	0/7	0/7	0/1	0/1		
	Min	23/8	3	2	2	1	0/3	0/2	0/3	0/0	0/0		
	Med	39/3	38/5	9	10/0	28	28/0	0/5	0/5	0/0	0/1		
	Range	86/2	87	18/0	18	89/0	35/8	0/4	0/4	0/1	0/1		
	Skew	2/25	0/217	0/312	0/4045	2/148	−0/95	−0/77	−0/108	1/80	0/035		

search terms [72].

$$\mathrm{MOA}\left(\mathrm{C_{Iter}}\right) = \mathrm{Min} + \mathrm{C_{Iter}} \times \left(\frac{\text{Max-Min}}{M_{\mathrm{Iter}}}\right) \tag{12}$$

The value of the function at the t^{th} iteration, as calculated by Eq. (12), is denoted as $\mathrm{MOA}\left(C_{\mathrm{Iter}}\right)$. The variable C_{Iter} represents the current iteration, which is a value between 1 and $\mathrm{M_{Iter}}$. The term "*Max*" represents the greatest value of this method, whereas "*Min*" represents the least value of this method.

The selection of the most fundamental principle was made in order to replicate the actions of arithmetic operators. This work proposes a set of location-updating calculations to be used throughout the exploration phase [72]:

$$X_{i,j}\left(C_{\mathrm{Iter}}+1\right) = \begin{cases} \mathrm{best}\left(\mathrm{x_j}\right) \div (\mathrm{MOP}+\varepsilon) \times \left(\left(\mathrm{UB_j}-\mathrm{LB_j}\right)\times\mu+\mathrm{LB_j}\right) \\ \qquad , \mathrm{r_2} < 0.5 \\ \mathrm{best}\left(\mathrm{x_j}\right) \times \mathrm{MOP} \times \left(\left(\mathrm{UB_j}-\mathrm{LB_j}\right)\times\mu+\mathrm{LB_j}\right) \\ \qquad , \text{Otherwise} \end{cases} \tag{13}$$

Based on the given equation, $X_i\left(C_{\mathrm{Iter}}+1\right)$ represents the $\mathrm{i_{th}}$ solution in the next iteration, $X_{i,j}\left(C_{\mathrm{Iter}}\right)$ represents the $\mathrm{j_{th}}$ position of the $\mathrm{i_{th}}$ solution in the current iteration, and best $\left(x_j\right)$ denotes the $\mathrm{j_{th}}$ position in the best obtained solution so far. The upper value of the $\mathrm{j_{th}}$ position is denoted as UB_j, whereas the lower value is denoted as LB_j. The symbol ε represents a small integer value. The symbol μ is a parameter of control that is used to alter the search strategy. Its value might be as low as 0.5 , relying on the specific topic being examined [72].

$$\mathrm{MOP}\left(C_{\mathrm{Iter}}\right) = 1 - \frac{C_{\mathrm{Iter}}^{1/\alpha}}{M_{\mathrm{Iter}}^{\alpha}} \tag{14}$$

In this equation, $\mathrm{MOP}\left(C_{\mathrm{Iter}}\right)$ signifies the function value at the t^{th} iteration, where Math Optimizer probability (MOP) indicates a coefficient. M_{Iter} and C_{Iter} show the iterations' maximum number and the present iteration. The exploitation precision across iterations is defined by α, set at 5 . In the current searching stage, the condition for the MOA function number corresponding to $r1$ is that it should not exceed the value of the present C_{Iter} (refer to Eq. (12)). The exploitation operators of the AOA algorithm is Subtraction (S) and Addition (A). In order to get a more refined predicted outcome, the exploration of the search area is conducted over several densely populated places, using two prominent search methodologies [72].

Table 4. The PPC values.

		Inputs				Output
		f_c	$d_{\max}$	CT	W/C	G_f
Inputs	f_c	1	-0.264	-0.218	-0.719	0.365
	$d_{\max}$	0.04409	1	0.142	0.277	0.374
	CT	0.47531	0.206	1	0.314	0.071
	W/C	-0.662	-0.035	-0.105	1	-0.302
Output	G_F	0.539	0.413	0.245	-0.317	1

$$X_{i,j}\left(C_{Iter}+1\right)= \begin{cases} best\left(x_j\right)-MOP\times\left(\left(UB_j-LB_j\right)\times\mu+LB_j\right) & r_3<0.5 \\ best\left(x_j\right)+MOP\times\left(\left(UB_j-LB_j\right)\times\mu+LB_j\right) & Otherwise \end{cases} \quad (15)$$

The *AOA* is a pioneering approach, and this study represents one of the first attempts to evaluate the efficacy of the *AOA* in quantifying damage.

3.3. Whale optimization algorithm (WOA)

During the migratory process, humpback whales engage in a behavior known as deep diving, when they descend to significant depths. Subsequently, they use a technique involving the creation of a spiral-shaped pattern of bubbles around their prey. Finally, the whales resurface and return to the ocean bottom [73]. They have a preference for preying on little fish that inhabit the vicinity of the ocean bottom. The mathematical model developed by *WOA* encompasses several aspects of the hunting behavior, including the encircling of the prey, the execution of spiral bubble operations, and the search process. The representation of the concept may be shown as follows:

3.3.1. The prey encircling

The *WOA* regards the identification of prey position as a potential candidate response. The below equations could be utilized to explain the humpback whales' encirclement [73]:

$$D=\left|C.X_p(t)-X(t)\right| \quad (16)$$

$$X(t+1)=X_p(t)-A.D \quad (17)$$

Based on these equations, t shows the present iteration, $X(t)$ indicates the location vector of whales, and $X_p(t)$ shows the location of the hunt A and C stand for coefficient vectors that can be computed as below [73]:

$$A=2\cdot ar-a \quad (18)$$

$$C=2.r \quad (19)$$

a is a gradually decreasing vector from 2 to 0 with a constant number of iterations, and r is an accidental vector between 0 and 1 .

3.3.2. Bubble attacking the prey

The act of attack exposes the *WOA* 's abuse of power or exploitation of local resources. The whales use two distinct approaches in their bubble net feeding strategy while engaging with their prey. The following expression is a mathematical representation:

1. The decreasing encircling mechanism is a hunting tactic used by whales, whereby they encircle their prey in progressively reducing rings. The task may be achieved by gradually decreasing the value of ' a ' from 2 to 0 , while ensuring that the absolute value of A remains less than 1.

2. The humpback whales exhibit a spiral pattern of movement as they ascend to their hunting grounds. The position of the whales may be updated using the formulae provided in reference [73]:

$$X(t+1)=D'.e^{bl}.\cos(2\pi l)+X_p(t) \quad (20)$$

$$D'=\left|X_p(t)-X(t)\right| \quad (21)$$

The above equations indicate that the variable 1 represents a real integer within the range of -1 to 1 , while the variable b represents a constant that characterizes the logarithmic helix shape.

During the course of the attack, the whales exhibit concurrent use of many methods. Consequently, it is anticipated that the encircling process will be reduced by 50% and the helix model will undergo a commensurate reduction in order to update their respective positions. This may be shown as shown below [73]:

$$X(t+1)=\begin{cases} X_p(t)-A.D & \text{if } p<0.5 \\ D'.e^{bl}\cos(2\pi l)+X_p(t) & \text{if } p\geq 0.5 \end{cases} \quad (22)$$

In this equation, p shows the possibility number $\in [1, 0]$.

3.3.3. *Searching for the prey*

The humpback whales look for a hunt throughout this procedure, representing the *WOA*'s exploration or worldwide search. The search procedure may be expressed by the $|A| > 1$. The location of the whales or spies may be modified as below [73]:

$$D = |C.X_r(t) - X(t)| \tag{23}$$

$$X(t+1) = X_r(t) - A.D \tag{24}$$

In Eqs. (23) and (24), $X_r(t)$ is an random vector of whale position (Fig. 2).

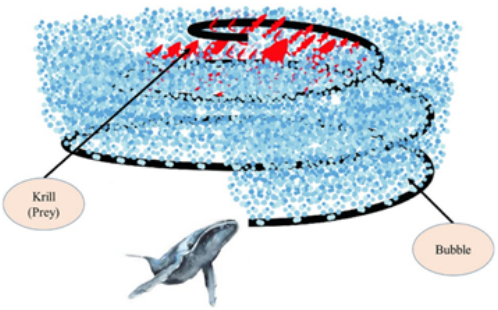

Fig. 2. The feeding outline of whales [73].

3.4. The trend of integration

For the purpose of developing models, the below outline was followed:

- First, the comprehensive dataset was produced from most related literatures.
- Second, pre-processing efforts have been performed on dataset, such as randomizing, removing bad data, and separating for train and test stages with normal distributions.
- At the third step, the initial SVR model was produced.
- Finally, the optimization algorithms were linked with SVR analysis to determine the optimal values of the hyperparameters of SVR(C, σ, and ε).

Figs. 3 and 4 illustrate the flowchart and process of the hybrid SVR analysis, which aims to utilize optimization algorithms to determine the optimal values for the determinative parameters of the SVR model.

4. Indices

The efficacy of the simulations was assessed by computing and analyzing several statistical criteria as described in Table 5.

5. Results

5.1. G_f

In this study, a specific portion of the data collection was used for the purpose of evaluating the G_f. This evaluation was conducted by using linked SVR networks that were upgraded by AOA and WOA. The objective of this inquiry was to develop distinct recommendation systems. To improve the modeling efficiency of the development, the AOA and WOA approaches were used to emphasize the model's crucial elements. As was previously indicated, the aim of SVR innovations was to provide a solution for the regulatory constants C, σ, and ε. The suggested parameters for computing SVR method features utilizing the AOA and WOA methods are shown in Table 6.

Analyzed and presented are the advantages of employing hybrid SVR algorithms to estimate the initial fracture energy $\left(G_f\right)$ of concrete. Calculations were employed in this case to calculate G_f by combining SVR with the AOA, WOA, and other approaches. The goal of the SVR ideas was to provide the most effective regulatory results. The concrete was isolated at random from a number of research papers for the phases of learning and evaluating. The comparison of the real and estimated G_f values, as well as the distribution of the ratio of Estimated/Real, are shown in Fig. 5. Utilizing five metrics $(R, R^2, RMSE, RRSE$, and VAF), the effectiveness of the existing techniques was evaluated. The findings on the $SVR - AOA$ and $SVR - WOA$ assessments are reported in Table 6. Both methods calculate the G_f, which assesses the intended correlation between the findings that are recorded and computed and the systems' long-term survivability.

The performance of the constructed regression evaluation models $SVR - AOA$ and $SVR-$ WOA's statistical metrics was evaluated in this portion of the essay to discover which model outperformed the others. Additionally, an effort was made to meaningfully compare the results of this

Table 5. Comparison of time performance and performance with different superpixel methods

Eq. No.	Description	Abv.	Formula
(25)	Correlation coefficient	R	$\frac{\sum_{R=1}^{R}(t_r-t)(y_r-\bar{y})}{\sqrt{\left[\sum_{r=1}^{R}(t_r-\mathrm{t})^2\right]\left[\sum_{r=1}^{R}(y_r-y)^2\right]}}$
(26)	Coefficient of determination	R^2	$\left(\frac{\sum_{r=1}^{R}(t_r-\bar{t})(y_r-\bar{y})}{\sqrt{\left[\sum_{r=1}^{R}(t_R-\mathrm{t})^2\right]\left[\sum_{r=1}^{R}(y_r-\bar{y})^2\right]}}\right)^2$
(27)	Root - mean - square error	$RMSE$	$\sqrt{\frac{1}{R}\sum_{\mathrm{r}=1}^{R}(y_\mathrm{r}-t_\mathrm{r})^2}$
(28)	Root Relative Squared Error	$RRSE$	$\sqrt{\frac{\sum_{r=1}^{R}(t_r-y_r)^2}{\sum_{r=1}^{R}(t_r-\bar{t})^2}}$
(29)	Variance account factor	VAF	$\left(1-\frac{\mathrm{var}(t_R-y_R)}{\mathrm{var}(t_R)}\right)*100$
	Terms:		
	t_d : The records		
	$\bar{t}$: The mean of records		
	y_d : The estimations		
	$\bar{y}$: The mean of estimations		
	R : Number of datasets		

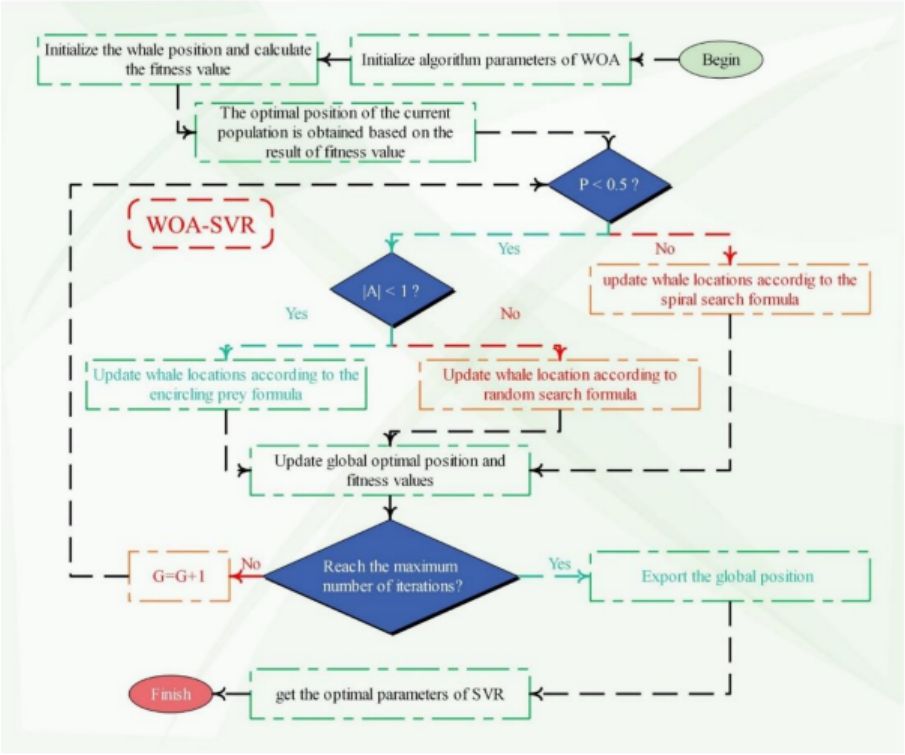

Fig. 3. The SVR - WOA flowchart.

study with those of earlier research. The calculations' findings, which included assessment factors, demonstrate that both $SVR-WOA$ and $SVR-AOA$ regression analyses can astonishingly operate, with R values of 0.92 and 0.9714 for $SVR-WOA$ and 0.9597 and 0.9926 for $SVR-AOA$, respectively, related to the train and test stages. The values of R^2 in the testing dataset's $SVR-WOA$ and $SVR-AOA$ regression analyses demonstrate the models' outstanding efficacy. To find the outperforming model, however, it is necessary to study and contrast the created indicators. The $SVR-AOA$ regression exhibits a decrease in the RMSE indicator value when compared to the $SVR-WOA$, going from 0.0055kN/m to 0.0035kN/m in the train portion. A reduction of 50%, from 0.0036kN/m to 0.0018kN/m,

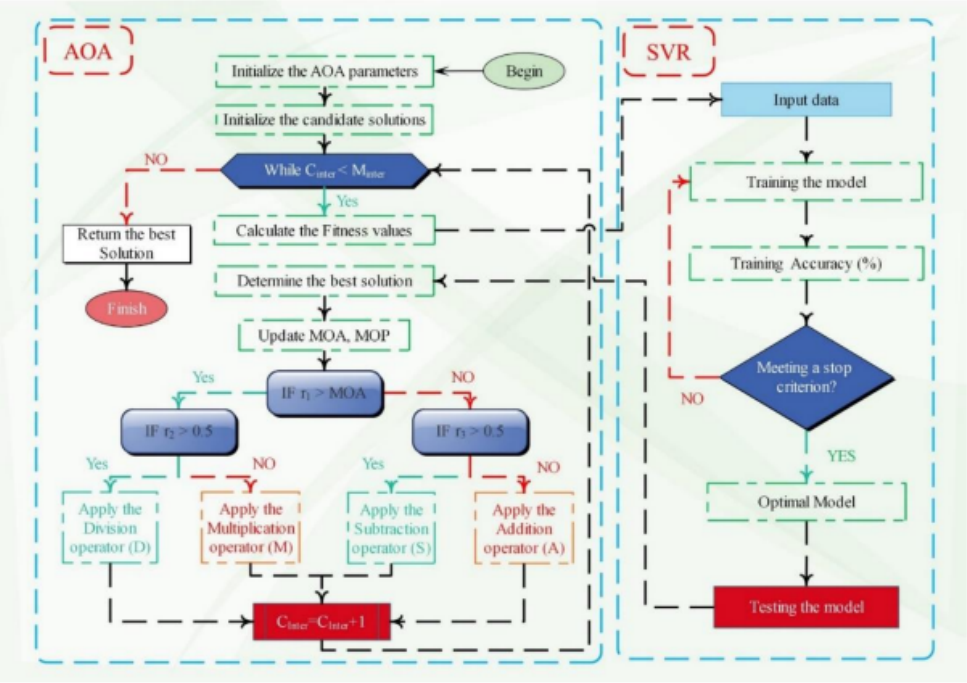

Fig. 4. The SVR - AOA flowchart.

was accomplished during the testing phase. The RRSE index has a similar trend to RMSE, suggesting that the values of this index for $SVR-AOA$ were much lower than $SVR-WOA$. This indicates that the $SVR-AOA$ network has more potential in accurately predicting process.

Moreover, the index VAF, which has been newly recognized, may also be used to illustrate the measured proficiency as shown in Table 6 (the higher value of VAF, the higher accuracy).

Similar large increases in the VAF index values can be seen in the learning phase (from 84.64% for $SVR-WOA$ to 92.07% for $SVR-AOA$) and the test portion (from 94.32% to 98.53%). To provide a foundation for comparison, the findings of this study were contrasted with those of a previous publication [26]. The $SVR-AOA$ regression created has an R-value rise from 0.95 to 0.9926 , which also results in a modest increase in effectiveness. Therefore, based on the reasoning and processability of the designs, it appears that the $SVR-AOA$ evaluation is highly reliable for establishing concrete G_f, even though the $SVR-WOA$ method has promise in the process of forecasting.

The error distribution plots in Fig. 5 demonstrate the ratio of predicted G_f to recorded G_f for $WOA-SVR$ and $AOA-SVR$. The more instances around ratio equal to one, and sharper distribution, the higher accuracy of model. As it is clear from figures, $AOA-SVR$ performs better than $WOA-SVR$ model in both training and testing stages by shaper distribution with more instances around ratio one.

5.2. G_F

In this study, a specific portion of the data collection was used for the purpose of evaluating the G_F. This evaluation was conducted by using linked SVR networks that were augmented by the AOA and WOA techniques. The objective of this inquiry was to develop distinct recommendation systems. The AOA and WOA techniques were chosen in order to emphasize the essential elements of the model, with the aim of enhancing the efficacy of its development. The suggested parameters for computing SVR approach characteristics using the AOA and WOA methods are shown in Table 7. The comparison of the real and estimated G_F values, as well as the histogram of the estimated/real ratio, are shown in Fig. 6.

This portion of the essay compares the results of the statistical signals produced for the constructed regression analyses known as $SVR-WOA$ and $SVR-AOA$ to see which model performed better than the others. Additionally, an effort was made to meaningfully compare the results of this study with those of earlier research. The results of the computations, show that both $SVR-WOA$ and $SVR-AOA$ analysis might astonishingly perform favorable during the prediction trendline, with R of 0.927 and 0.9278 for

Table 6. The efficiency of the SVR for calculating G_f.

Category	Index	Hyperparameter	System		[26]
			$SVR-WOA$	$SVR-AOA$	
		C	470.226	826.26	
		σ	0.56411	0.9833	
		ε	0.1022	0.1	
Train	R		0/92	0/9597	
	R^2		0/8465	0/921	
	RMSE		0/0055	0/0035	
	RRSE		0/4467	0/2824	
	VAF		84/648	92/0699	
Test	R		0/9714	0/9926	0/95
	R^2		0/9437	0/9853	
	RMSE		0/0036	0/0018	
	RRSE		0/2615	0/1268	
	VAF		94/3238	98/5271	

Table 7. The results of the SVR models.

		Hyperparameter	System		[26]
			$SVR-WOA$	$SVR-AOA$	
Stage	Metrics	C	470.226	922.288	
		σ	0.3634	0.757	
		ε	0.1	0.1	
Train	R		0/927	0/9634	0.91
	R^2		0/8594	0/9281	
	$RMSE$		0/0157	0/0074	
	$RRSE$		0/5666	0/2682	
	VAF		85/905	92/8082	
Test	R		0/9278	0/961	
	R^2		0/8608	0/9236	
	$RMSE$		0/0155	0/0078	
	$RRSE$		0/5556	0/2793	
	VAF		86/0723	92/2014	

$WOA-SVR$, and 0.9634 and 0.961 for $SVR-AOA$, respectively, for the train and test stage. To identify the top-performing model, however, it is necessary to assess and contrast the produced indicators. The $SVR-AOA$ regression exhibits a decrease in the $RMSE$ index value when compared to the $SVR-WOA$, going from 0.0157kN/m to 0.0074kN/m in the train portion. A reduction of 50%, from 0.0155kN/m to 0.0078kN/m, was accomplished during the testing phase. The $RRSE$ index has a similar trend to $RMSE$, suggesting that the values of this index for $SVR-AOA$ were much lower than $SVR-WOA$. This implies that the $SVR-AOA$ network has greater promise in predicting the G_F. Both the learning and test portions of the VAF

values significantly improved, going from 86.07% to 92.2% for the test portion and from 85.9% for $WOA-SVR$ to 92.81% for $SVR-AOA$. To provide a foundation for comparison, the findings from this paper were contrasted with those from a previous publication [26]. The $SVR-AOA$ regression created has an R-value rise from 0.91 to 0.9634 , which also results in a modest increase in effectiveness. As a result, despite the $SVR-WOA$ system's capability for prediction, the $SVR-AOA$ analysis appears to be fairly trustworthy for determining concrete G_F, according to the justifications and processability of the systems.

Fig. 6 displays the error distribution plots, which illustrate the ratio between the anticipated G_F and the observed G_F for both $WOA-SVR$ and $AOA-SVR$. A better level of accuracy in a model is achieved when there is a greater frequency of cases with a ratio equal to one, as well as a more pronounced dispersion. Based on the presented data, it is evident that the $AOA-SVR$ model outperforms the $WOA-SVR$ model in both the training and testing phases. This superiority is shown by a more pronounced distribution, with a higher concentration of cases around the ratio of one.

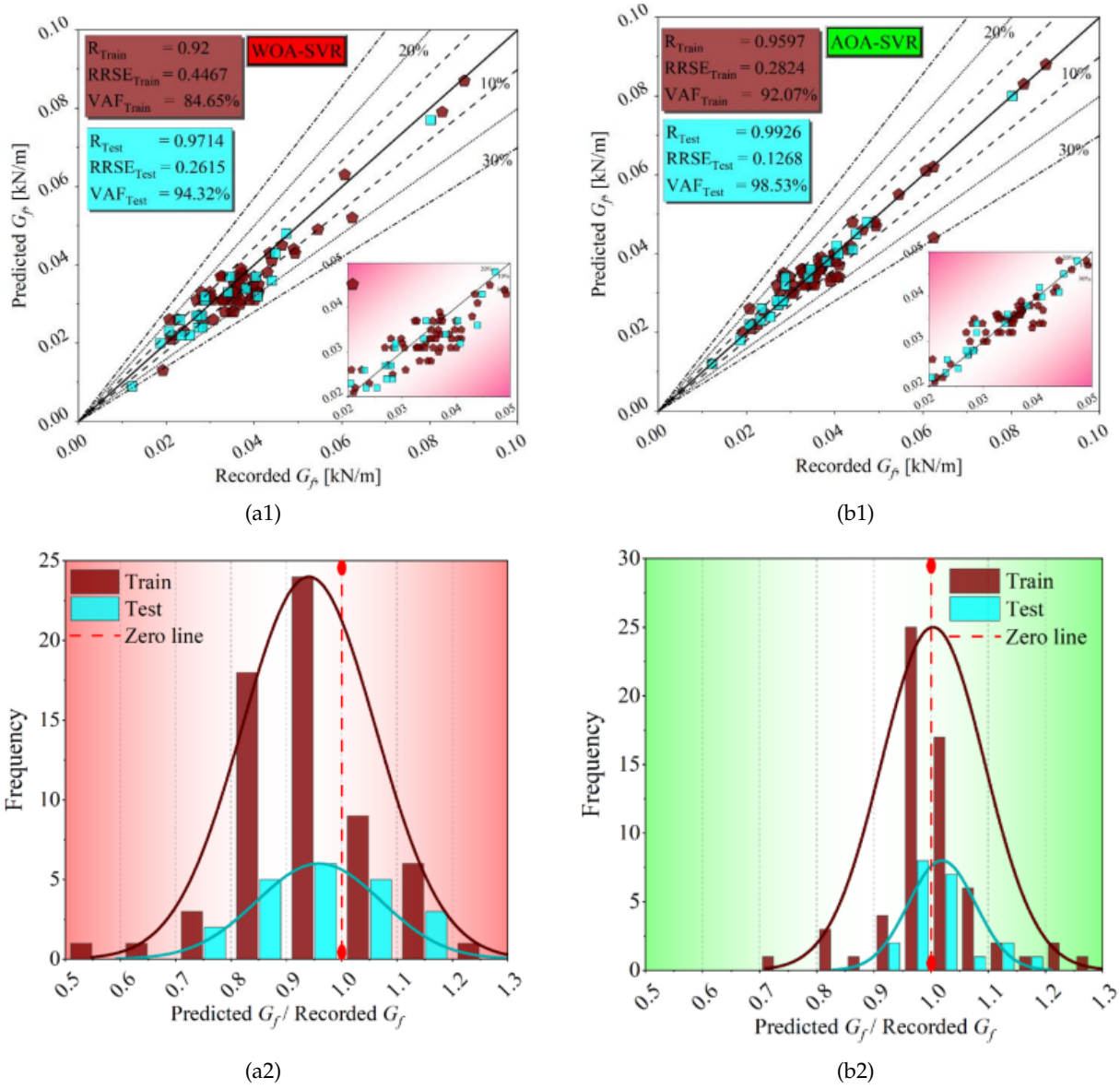

Fig. 5. The models' results.

6. Conclusion

This study created a coupled SVR methodology to have a greater performance of concrete's initial $\left(G_f\right)$ and total fracture energy (G_F). Systems were utilized to estimate the G_f and G_F in this situation by integrating the arithmetic optimization algorithm (AOA) and whale optimization algorithm (WOA) approaches with SVR. For this experiment, a data set was created that includes four data inputs and two outcome factors. At last, the performance of models has compared altogether and literature by calculating and analyzing different statistical criteria.

- Considering G_f, the findings of the calculations show that both $SVR-WOA$ and $SVR-AOA$ might perform favorable via the estimation outline, with R of 0.92 and 0.9714 for $SVR-WOA$, and 0.9597 and 0.9926 for $SVR-AOA$, respectively, for the train and test stage. The models' wonderful performance is supplied in the values of R^2 in both SVR WOA and $SVR-AOA$ regression analysis in the testing dataset. Related to RMSE index, the $SVR-AOA$ depicted a decline in comparison to the $SVR-WOA$, coming from 0.0055kN/m to 0.0035kN/m in the training stage. With an increment in R-value from 0.95 [26] to 0.9926 , the created $SVR-AOA$ also reported a good modification in usefulness.

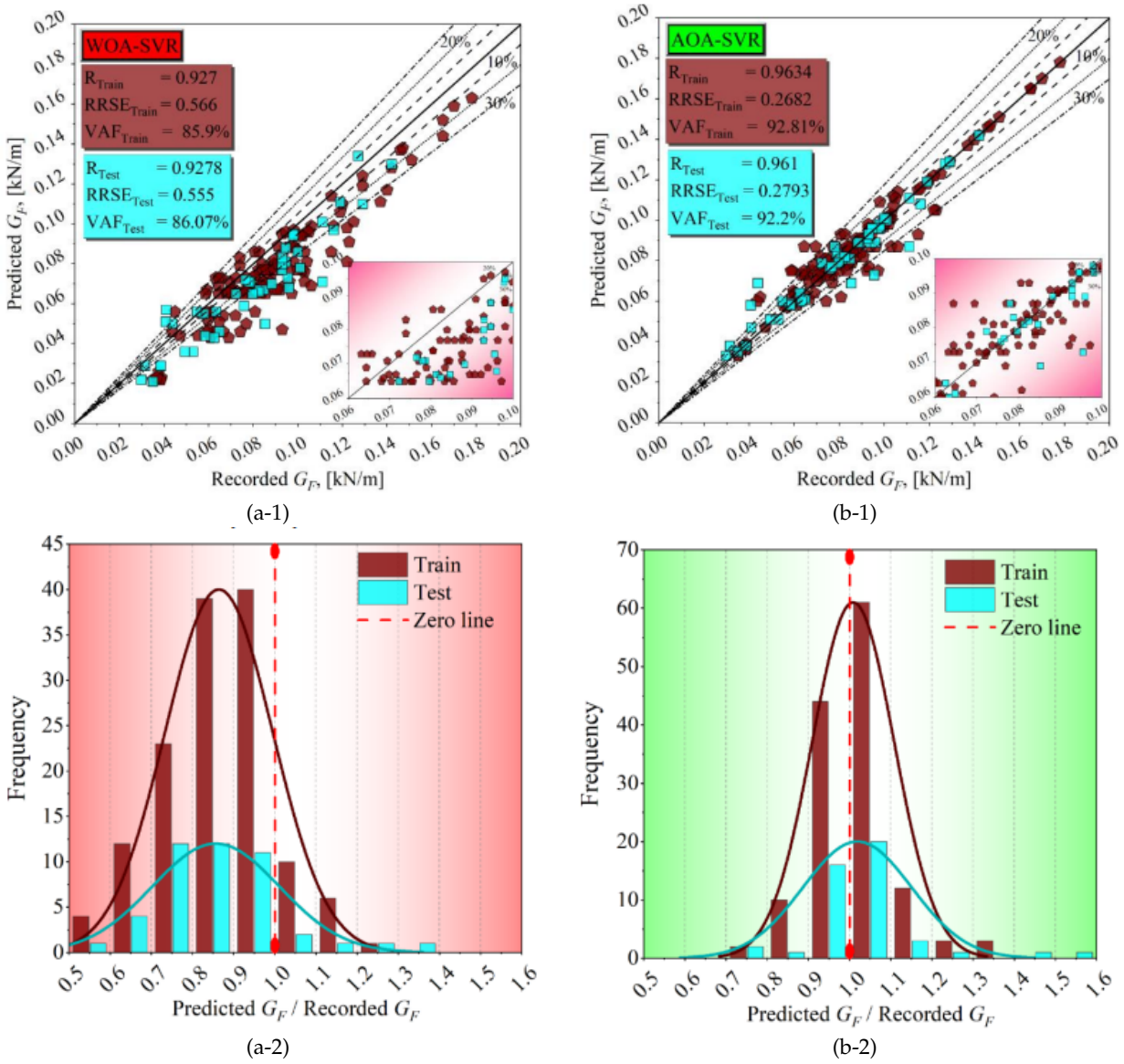

Fig. 6. The results of models.

- Regarding G_F, the findings of the calculations depicted that both $SVR-WOA$ and SVR - AOA might remarkably perform with favorable via the outline, with R of 0.927 and 0.9278 for $SVR-WOA$, and 0.9634 and 0.961 for $SVR-AOA$, respectively, related to the train and test stages. Related to $RMSE$, the $SVR-AOA$ depicts a decline compared to the $SVR-WOA$. For test portion, a half decline from 0.0155kN/m to 0.0078kN/m was founded. The values of the VAF supplied a good increment in the train stage, from 85.9% for $WOA-SVR$ to 92.81% for $SVR-AOA$. The resulting $SVR-AOA$ model likewise offers an excellent boost in effectiveness with a rise in R value from 0.91 [26] to 0.9634.

- As it was clear from error distribution plots for G_f and G_F, $AOA-SVR$ performs better than $WOA-SVR$ model in both training and testing stages by shaper distribution with more instances around Predicted / Recorded ratio equals to one.

- The regression models that have been constructed possess the capability to be practically used in the determination of concrete fracture energy. The precise estimation of G_f and G_F has the potential to enhance the optimization of concrete design and the evaluation of the structural soundness of concrete components, hence

making a valuable contribution to the advancement of construction methodologies. The study included a total of 264 samples that were obtained from previous research endeavors. The addition of this database proved to be beneficial in the development of the regression systems. However, it is worth noting that the inclusion of a bigger and more varied dataset has the potential to improve the generalizability and dependability of these models. In order to enhance the generalizability and reliability of the regression simulations, it would be advantageous to gather a bigger and more varied dataset. The integration of data from diverse sources and the incorporation of varied concrete compositions and mechanical aspects have the potential to increase the prediction capacities of the models. Performing a comparison study with other regression approaches that are often used for the prediction of fracture energy will provide a more comprehensive comprehension of the merits and limitations of the suggested models. The application of the created models to real-world circumstances and the subsequent validation of their performance on actual physical structures would constitute a crucial milestone in the practical implementation process.

- Therefore, despite the potential of the $SVR - WOA$ framework for the process of forecasting, the $SVR - AOA$ assessment appears to be a reliable method for determining concrete G_f and G_F. This conclusion is based on the logic and processability of the models.

Acknowledgment

This work was supported Research Project of Cangzhou City Social Development "Research on the application of BIM technology in smart buildings under the background of smart city construction", (No.2022089).

References

[1] R. Ince, (2012) *"Determination of concrete fracture parameters based on peak-load method with diagonal split-tension cubes"* **Engineering Fracture Mechanics *82***: 100–114.

[2] S. Dehghan, *"Comparison of seismic behavior factors for reinforced concrete (RC) special moment resisting frames (SMRFs) in Iran in low-, mid-, and high-rise buildings based on Iranian seismic standard 2800 and ASCE"*:

[3] Z. P. Bažant and E. Becq-Giraudon, (2002) *"Statistical prediction of fracture parameters of concrete and implications for choice of testing standard"* **Cement and concrete research *32***: 529–556.

[4] M. F. Kaplan. "Crack propagation and the fracture of concrete". In: ***58***. 1961, 591–610.

[5] C. E. Kesler, D. J. Naus, and J. L. Lott. "Fracture mechanics-its applicability to concrete". In: 1972.

[6] A. Hillerborg, M. Modéer, and P.-E. Petersson, (1976) *"Analysis of crack formation and crack growth in concrete by means of fracture mechanics and finite elements"* **Cement and concrete research *6***: 773–781.

[7] Y. Jenq and S. P. Shah, (1985) *"Two parameter fracture model for concrete"* **Journal of engineering mechanics *111***: 1227–1241.

[8] G. V. Guinea, J. Planas, and M. Elices, (1992) *"Measurement of the fracture energy using three-point bend tests: Part 1—Influence of experimental procedures"* **Materials and Structures *25***: 212–218.

[9] N. Trivedi, R. K. Singh, and J. Chattopadhyay, (2015) *"Investigation on fracture parameters of concrete through optical crack profile and size effect studies"* **Engineering Fracture Mechanics *147***: 119–139.

[10] J. Planas, M. Elices, and G. V. Guinea, (1992) *"Measurement of the fracture energy using three-point bend tests: Part 2—Influence of bulk energy dissipation"* **Materials and Structures *25***: 305–312.

[11] R. A. Einsfeld and M. S. L. Velasco, (2006) *"Fracture parameters for high-performance concrete"* **Cement and Concrete Research *36***: 576–583.

[12] Y. Dawei, Z. Bing, G. Bingbing, G. Xibo, and B. Razzaghzadeh, (2023) *"Predicting the CPT-based pile set-up parameters using HHO-RF and PSO-RF hybrid models"* **Structural Engineering and Mechanics *86***: 673–686.

[13] G. Moradi, E. Hassankhani, and A. M. Halabian, (2022) *"Experimental and numerical analyses of buried box culverts in trenches using geofoam"* **Proceedings of the Institution of Civil Engineers-Geotechnical Engineering *175***: 311–322.

[14] B. Bayrami, (2022) *"Estimation of splitting tensile strength of modified recycled aggregate concrete using hybrid algorithms"* **Available at SSRN 3992623**:

[15] R. S. Benemaran and M. Esmaeili-Falak, (2023) *"Predicting the Young's modulus of frozen sand using machine learning approaches: State-of-the-art review"* **Geomechanics and Engineering *34***: 507–527.

[16] M. K. Amiri, S. P. G. Zaferani, M. R. S. Emami, S. Zahmatkesh, R. Pourhanasa, S. S. Namaghi, J. J. Klemeš, A. Bokhari, and M. Hajiaghaei-Keshteli, (2023) *"Multi-objective optimization of thermophysical properties GO powders-DW/EG Nf by RSM, NSGA-II, ANN, MLP and ML"* **Energy**: 128176.

[17] M. Esmaeili-Falak and R. S. Benemaran, (2023) *"Ensemble deep learning-based models to predict the resilient modulus of modified base materials subjected to wet-dry cycles"* **Geomechanics and Engineering *32***: 583–600.

[18] A. R. Nasab and H. Elzarka, (2023) *"Optimizing Machine Learning Algorithms for Improving Prediction of Bridge Deck Deterioration: A Case Study of Ohio Bridges"* **Buildings *13***: 1517.

[19] R. S. Benemaran, M. Esmaeili-Falak, and A. Javadi, (2022) *"Predicting resilient modulus of flexible pavement foundation using extreme gradient boosting based optimised models"* **International Journal of Pavement Engineering**: 1–20.

[20] X. Shi, X. Yu, and M. Esmaeili-Falak, (2023) *"Improved arithmetic optimization algorithm and its application to carbon fiber reinforced polymer-steel bond strength estimation"* **Composite Structures *306***: 116599.

[21] R. S. Benemaran, (2023) *"Application of extreme gradient boosting method for evaluating the properties of episodic failure of borehole breakout"* **Geoenergy Science and Engineering *226***: 211837.

[22] S. Roudini, L. C. Murdoch, M. Shojaei, and S. DeWolf, (2023) *"Proxy-based Bayesian inversion of strain tensor data measured during well tests"* **Geomechanics for Energy and the Environment *36***: 100506.

[23] M. Esmaeili-Falak, H. Katebi, M. Vadiati, and J. Adamowski, (2019) *"Predicting triaxial compressive strength and Young's modulus of frozen sand using artificial intelligence methods"* **Journal of Cold Regions Engineering *33***: 04019007.

[24] M. Khorshidi, A. Goli, M. Orešković, K. Khayambashi, and M. Ameri, (2023) *"Performance evaluation of asphalt mixtures containing different proportions of alternative materials"* **Sustainability *15***: 13314.

[25] E. Tabasi, B. Jahangiri, and F. Kooban, (0) *"Effect of temperature profile on dynamic behaviour of asphalt pavements under moving loads"* **Proceedings of the Institution of Civil Engineers - Construction Materials *0***(0): 1–16. DOI: 10.1680/jcoma.22.00116.

[26] I. Afshoon, M. Miri, and S. R. Mousavi, (2021) *"Combining Kriging meta models with U-function and K-Means clustering for prediction of fracture energy of concrete"* **Journal of Building Engineering *35***: 102050.

[27] Z. Wang, (2023) *"Integrated and optimized SVR analysis: Assessment of the preliminary and entire fracture energy of concrete"* **Journal of Intelligent & Fuzzy Systems**: 1–18.

[28] M. J. G. Rad, S. Ohadi, J. Jafari-Asl, A. Vatani, S. A. Ahmadabadi, and J. A. F. O. Correia. "GNDO-SVR: An efficient surrogate modeling approach for reliability-based design optimization of concrete dams". In: ***35***. Elsevier, 2022, 722–733.

[29] K. Khan, M. Iqbal, R. Biswas, M. N. Amin, S. Ali, J. Gudainiyan, A. A. Alabdullah, and A. M. A. Arab, (2022) *"A Hybrid SVR-Based Prediction Model for the Interfacial Bond Strength of Externally Bonded FRP Laminates on Grooves with Concrete Prisms"* **Polymers *14***: 3097.

[30] H. U. Ahmed, R. R. Mostafa, A. Mohammed, P. Sihag, and A. Qadir, (2023) *"Support vector regression (SVR) and grey wolf optimization (GWO) to predict the compressive strength of GGBFS-based geopolymer concrete"* **Neural Computing and Applications *35***: 2909–2926.

[31] C. Fan, Y. Zheng, S. Wang, and J. Ma, (2023) *"Prediction of bond strength of reinforced concrete structures based on feature selection and GWO-SVR model"* **Construction and Building Materials *400***: 132602.

[32] M. S. Alam, N. Sultana, and S. M. Z. Hossain, (2021) *"Bayesian optimization algorithm based support vector regression analysis for estimation of shear capacity of FRP reinforced concrete members"* **Applied Soft Computing *105***: 107281.

[33] M. R. Kaloop, B. Roy, K. Chaurasia, S.-M. Kim, H.-M. Jang, J.-W. Hu, and B. S. Abdelwahed, (2022) *"Shear strength estimation of reinforced concrete deep beams using a novel hybrid metaheuristic optimized SVR models"* **Sustainability *14***: 5238.

[34] Y. Peng and C. Unluer, (2023) *"Modeling the mechanical properties of recycled aggregate concrete using hybrid machine learning algorithms"* **Resources, Conservation and Recycling *190***: 106812.

[35] S. S. Zadeh, N. Joushideh, B. Bahrami, and S. Niyafard, (2023) *"A review on concrete recycling"* **World Journal of Advanced Research and Reviews *19***: 784–793.

[36] C. E.-I. du Béton. *CEB-FIP model code 1990: Design code*. Thomas Telford Publishing, 1993.

[37] C. F. Code, (2010) *"model (2010) Fib model code for concrete structures 2010"* **Doc Competence Cent Siegmar Kästl eK, Ger**:

[38] J. C. Committee, (2007) *"Standard Specifications for Concrete Structures—2007"* **Japan Society of Civil Engineers: Tokyo, Japan**:

[39] M. Khorshidi, M. Ameri, and A. Goli, (2023) *"Cracking performance evaluation and modelling of RAP mixtures containing different recycled materials using deep neural network model"* **Road Materials and Pavement Design**: 1–20.

[40] M. H. Basiri, F. Javadnejad, and A. Saeidi. "Forecasting crude oil price with an artificial neural network model based on a regular pattern for selecting training and testing sets using dynamic command-line functions". In: 2015.

[41] M. Malmir, H. Momeni, and A. Ramezani. "Controlling megawatt class WECS by ANFIS network trained with modified genetic algorithm". In: IEEE, 2019, 939–943.

[42] X. Wang, H. A. Saifullah, H. Nishikawa, and K. Nakarai, (2020) *"Effect of water–cement ratio, aggregate type, and curing temperature on the fracture energy of concrete"* **Construction and Building Materials *259***: 119646.

[43] D. Darwin, S. Barham, R. Kozul, and S. Luan. "Fracture energy of high-strength concrete". In: American Concrete Institute, 2001.

[44] F. H. Wittmann, P. E. Roelfstra, H. Mihashi, Y.-Y. Huang, X.-H. Zhang, and N. Nomura, (1987) *"Influence of age of loading, water-cement ratio and rate of loading on fracture energy of concrete"* **Materials and structures *20***: 103–110.

[45] T.-P. Chang and M.-M. Shieh, (1996) *"Fracture properties of lightweight concrete"* **Cement and concrete research *26***: 181–188.

[46] K. M. El-Sayed, G. V. Guinea, C. Rocco, J. Planas, and M. Elices. "Influence of aggregate shape on the fracture behaviour of concrete, Fracture Mechanics of Concrete Structures". In: 1998.

[47] R. Gettu, Z. P. Bazant, and M. E. Karr, (1990) *"Fracture properties and brittleness of high-strength concrete."* **ACI Materials Journal *87***: 608–618.

[48] M. Hassanzadeh, (1998) *"The influence of the type of coarse aggregates on the fracture mechanical properties of high-strength concrete"* **AEDIFICATIO Publishers, Fracture Mechanics of Concrete Structures, *1***: 161–170.

[49] H. K. Hilsdorf and W. Brameshuber. *Size effects in the experimental determination of fracture mechanics parameters*. 1985.

[50] Y. S. Jenq and S. P. Shah, (1985) *"A fracture toughness criterion for concrete"* **Engineering fracture mechanics *21***: 1055–1069.

[51] R. John and S. P. Shah. *EFFECT OF HIGH STRENGTH AND RATE OF LOADING ON FRACTURE PARAMETERS OF CONCRETE*. 1987.

[52] B. L. Karihaloo and P. Nallathambi, (1989) *"Fracture toughness of plain concrete from three-point bend specimens"* **Materials and structures *22***: 185–193.

[53] L. J. Malvar and G. E. Warren, (1988) *"Fracture energy for three-point-bend tests on single-edge-notched beams"* **Experimental Mechanics *28***: 266–272.

[54] S. Mindess, (1984) *"The effect of specimen size on the fracture energy of concrete"* **Cement and Concrete Research *14***: 431–436.

[55] P.-E. Petersson. *Crack growth and development of fracture zones in plain concrete and similar materials*. 1981.

[56] C. Sok, J. Baron, and D. Francois, (1979) *"Mecanique de la rupture appliquee au beton hydraulique"* **Cement and Concrete Research *9***: 641–648.

[57] P. C. Strange and A. H. Bryant, (1979) *"Experimental tests on concrete fracture"* **Journal of the Engineering Mechanics Division *105***: 337–342.

[58] T. Tang, C. Ouyang, and S. P. Shah, (1996) *"Simple method for determining material fracture parameters from peak loads"* **Materials Journal *93***: 147–157.

[59] A. Ghaemmaghami and M. Ghaemian, (2006) *"Large-scale testing on specific fracture energy determination of dam concrete"* **International Journal of Fracture *141***: 247–254.

[60] W. C. Tang and T. Y. Lo, (2009) *"Mechanical and fracture properties of normal-and high-strength concretes with fly ash after exposure to high temperatures"* **Magazine of Concrete Research *61***: 323–330.

[61] S. P. Shah, C. Ouyang, S. Marikunte, W. Yang, and E. Becq-Giraudon, (1998) *"A method to predict shrinkage cracking of concrete"* **Materials Journal *95***: 339–346.

[62] B. H. Bharatkumar, B. K. Raghuprasad, D. S. Ramachandramurthy, R. Narayanan, and S. Gopalakrishnan, (2005) *"Effect of fly ash and slag on the fracture characteristics of high performance concrete"* **Materials and Structures *38***: 63–72.

[63] B.-J. Yu and F. Ansari, (1996) *"Method and theory for nondestructive determination of fracture energy in concrete structures"* **Structural Journal *93***: 602–613.

[64] A. Carpinteri, (1981) *"Experimental determination of fracture toughness parameters KIC and JIC for aggregative materials"* **Advances in fracture research *4***: 1491–1498.

[65] Z. P. Bazant and P. A. Pfeiffer, (1987) *"Determination of fracture energy from size effect and brittleness number"* **ACI Materials Journal *84***: 463–480.

[66] G. A. Rao and B. K. R. Prasad, (2002) *"Fracture energy and softening behavior of high-strength concrete"* **Cement and Concrete Research *32***: 247–252.

[67] S. N. N. Iravani and P. D. R. S. Ahd, (2021) *"Investigation of Retrofitting Reinforced Concrete Structures in Near-Fault Regions"* **Turkish Journal of Computer and Mathematics Education (TURCOMAT) *12***: 7729–7738.

[68] S. Roudini, L. C. Murdoch, M. Shojaei, and S. DeWolf, (2023) *"Proxy-based Bayesian inversion of strain tensor data measured during well tests"* **Geomechanics for Energy and the Environment *36***: 100506.

[69] V. N. Vapnik, (1999) *"An overview of statistical learning theory"* **IEEE transactions on neural networks *10***: 988–999.

[70] M. Aghayari Hir, M. Zaheri, and N. Rahimzadeh, (2023) *"Prediction of Rural Travel Demand by Spatial Regression and Artificial Neural Network Methods (Tabriz County)"* **Journal of Transportation Research *20***(4): 367–386. DOI: 10.22034/tri.2022.312204.2970.

[71] J. A. K. Suykens, J. D. Brabanter, L. Lukas, and J. Vandewalle, (2002) *"Weighted least squares support vector machines: robustness and sparse approximation"* **Neurocomputing *48***: 85–105.

[72] L. Abualigah, A. Diabat, S. Mirjalili, M. A. Elaziz, and A. H. Gandomi, (2021) *"The arithmetic optimization algorithm"* **Computer methods in applied mechanics and engineering *376***: 113609.

[73] S. Mirjalili and A. Lewis, (2016) *"The whale optimization algorithm"* **Advances in engineering software *95***: 51–67.